Nonlinear Vibration Tests of Isotropic Cylindrical Shells under Compressive Axial Loads

L.Gunawan[1] A.W.H.Klompé[2] R.J.Zwaan[3]

Delft University of Technology
Faculty of Aerospace Engineering
Kluyverweg 1, 2629 HS Delft, The Netherlands

Abstract

Vibration tests of thin-walled aluminium cylindrical shells were performed to validate theoretical analysis methods. For this purpose a vibration test setup was built with noncontacting excitation and response measurement systems. In the development of the setup the main attention was paid to the design of the excitation system which consists of two self-built acoustic drivers and a pressure synchronizer. Two capacitive displacement transducers were used to measure shell responses which were positioned at two circumferential positions. This enabled the measurement of traveling waves. The test setup was placed in a compression test bench. With this test setup the vibration tests were performed for several compressive load levels and excitation levels. The results showed the known phenomena which were predicted by the analysis methods and were observed in earlier experiments. Other phenomena which are not modelled in the analysis methods were also detected.

1. Introduction

Cylindrical shell structures employed in aerospace structures are often forced to vibrate at a high response level. The vibrations may disturb the proper functioning of other systems in the spacecraft and even may cause severe damage. To suppress these vibrations or to reduce them to an acceptable level their characteristics must be understood.

Extensive studies have been performed on vibrations of shells with various kinds of materials and structure, from isotropic to anisotropic ones. At low response levels the vibration characteristics, i.e. the natural frequencies and corresponding mode shapes can be predicted with the linearized governing equations. Various parameters which affect the natural frequencies have been identified, such as boundary conditions, axial loads, and geometric imperfections. At large response levels the nonlinear terms in the governing equations can not be neglected and hence the analysis has to be carried out in a more complicated manner.

At the Delft University of Technology an extensive program is carried out in which buckling and vibrations of thin cylindrical shells under compressive loads and with imperfections are being studied by theoretical analysis. Despite the progress made, not many vibration experiments have been done as yet [16]. To validate the theoretical analysis of nonlinear vibrations of cylindrical shells [5, 15], experiments on isotropic shell vibrations were carried out. This paper presents and discusses the test setup and some results of the vibration tests. The observed nonlinear response behavior is compared with the theoretical results.

2. Analyses Review

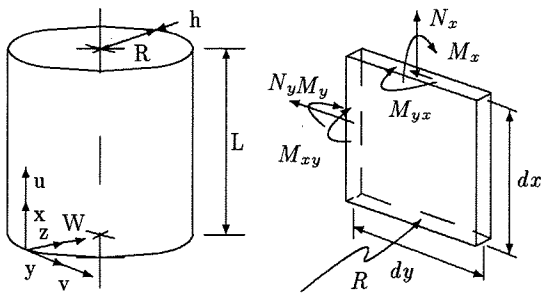

Symbol	Boundary Conditions			
SS3	W=0	M_x=0	v=0	N_x=0
C4	W=0	$W_{,x}$=0	v=0	u=0

Figure 1: Definition of shell geometry and boundary conditions

Figure 1 shows the geometry and the coordinate system of a cylindrical shell, where the curvilinear coordinates x, y, z and the corresponding dis-

[1]Graduate student, Ph.D.candidate
[2]Scientific staff member
[3]Professor of Aircraft Vibrations and Aeroelasticity

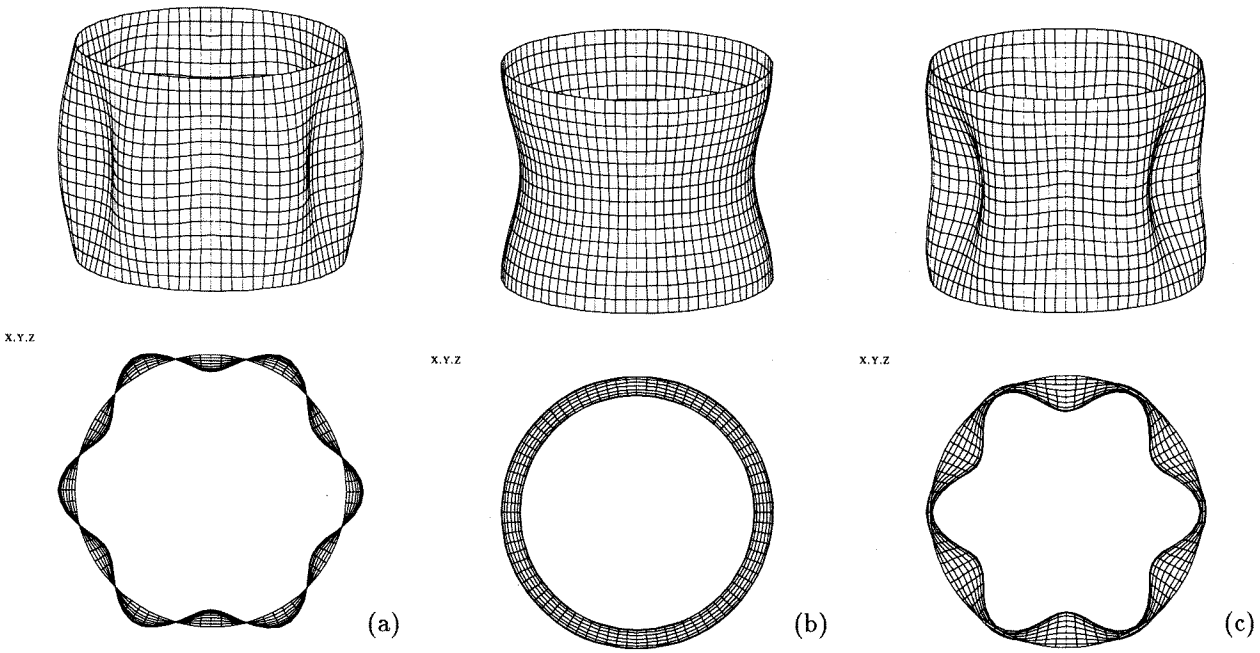

Figure 2: Vibration modes of cylindrical shells. (a) For linear analysis, (b) The shell contraction term, and (c) The nonlinear analyses

placements u, v, and W are shown in their positive directions. The boundary conditions which describe the displacements and the stresses are listed in the corresponding table (SS3=simply supported, C4=clamped).

The Governing Equations

The geometry of the shells introduce nonlinear relationships between the components of strain and deformation. Donnel's shallow shell theory is used in the analysis, which is sufficiently accurate for deformation patterns with a number of full waves in circumferential direction larger than 4. The in-plane inertias and damping forces are neglected in the formulation for simplicity.

The governing equations for an isotropic shell are the compatibility between strain and deformation:

$$\frac{1}{Eh}\nabla^4 F = -\frac{1}{R}W_{,xx} - \frac{1}{2}L_{NL}(W, W+2\bar{W}) \qquad (1)$$

and the equilibrium of forces in radial direction:

$$\frac{Eh^3}{12(1-\nu^2)}\nabla^4 W = \frac{1}{R}F_{,xx} + L_{NL}(F, W+\bar{W}) + p - \bar{\rho}hW_{,tt}\,, \qquad (2)$$

where E is Young's modulus, ν is Poisson's ratio, ∇^4 is the two-dimensional biharmonic operator, F is the Airy stress function, $\bar{W}$ is the initial geometric imperfections function.

Modelling of the Response

The analysis was carried out by introducing displacement functions in the governing equations. The vibration modes used in the linear analyses of cylindrical shell are:

$$W = A(x,t)\cos\frac{ly}{R} \qquad (3)$$

where l is the number of circumferential full waves and $A(x,t)$ is a function of axial position x which depends on the boundary conditions and time t. **Figure 2.a** illustrates the mode shape of a shell with SS3-SS3 boundary conditions. The term A(x,t) in equation 3 for this case is $A(t)\sin m\pi x/L$ with m is the axial half waves number. The figure shows mode shape for m=1 and l=6 which further referred as mode (1,6).

The analysis of large amplitude shell vibrations by using nonlinear theories with the modes described in equation 3 resulted in the conclusions that the nonlinearity is strong and of a hardening type [4, 18]. This, however, was not confirmed by some observations. Another mode that describes the contraction of the shell is introduced in addition to the first mode following the formulation of Evensen [6]. The extended response model is given by the following equation:

$$W = A(x,t)\cos\frac{ly}{R} + C(x,t) \qquad (4)$$

Figure 2.b illustrates the contraction mode, which for the SS3-SS3 shell is $C(t)\sin^2 m\pi x/L$, and

figure 2.c the extended mode shape. The frequency of the contraction mode is twice as much as that of the flexural bending mode, as shown in **figure 3**. By using this additional mode, the analysis resulted in a softening nonlinearity.

Another phenomenon predicted and observed in the experiments is the occurrence of traveling waves although the excitation forces were configured to drive only the standing waves. This indicated that another mode which is identical to the directly excited mode contributes in the response due to the nonlinear coupling, and that the "coupled" mode has 90 deg phase difference in time with respect to the directly driven mode. To take account of this phenomena in the analysis, another term is introduced in the response model, yielding:

$$W = A(x,t)\cos\frac{ly}{R} + B(x,t)\sin\frac{ly}{R} + C(x,t) \qquad (5)$$

Figure 4 illustrates the modelling of the traveling wave response as contribution of two identical mode with phase difference principally 90 deg in space and time.

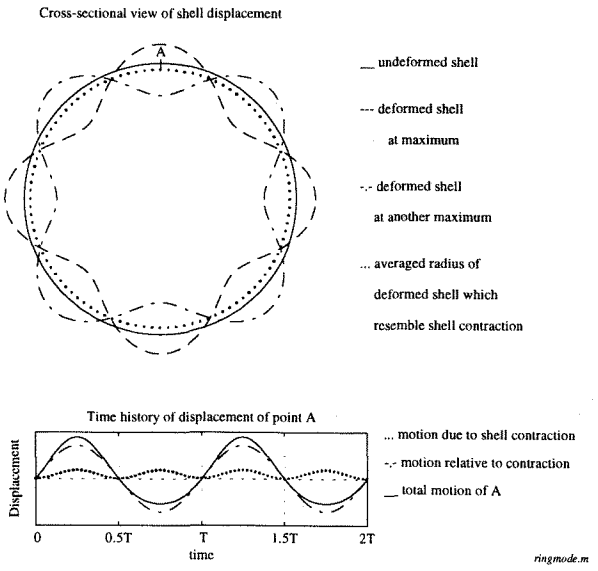

Figure 3: Cross sectional view of the nonlinear vibration modes. The time history plot shows that the axisymmetric term oscillates twice the frequency of the asymmetric term

Results of Analysis

By using the response model of equation 5, the analysis shows resonance response of the driven mode with a weak softening nonlinearity. Within a certain frequency range around resonance, the companion mode contributes in the response due to nonlinear coupling

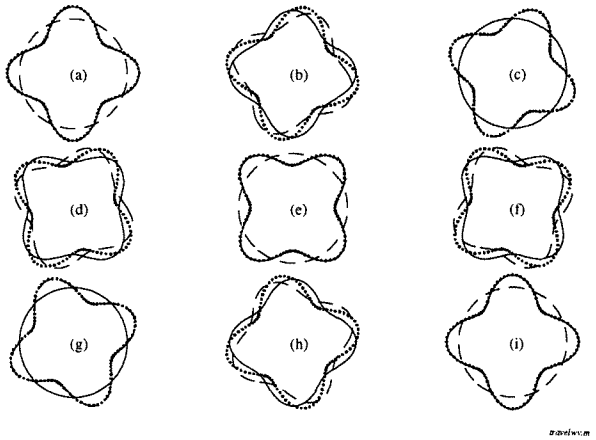

Figure 4: The traveling waves response as combination of two independent modes which differ 90 deg in circumferential position and time. The solid lines are the driven mode, the dashed lines are the companion mode, and the dotted lines are the total response

and the amplitude of the companion mode can be as high as that of the driven mode.

The presence of axial loads shifts the natural frequencies to lower values. They do not change the nonlinear behavior of the response however they may affect the stability of the response.

3. Experiment

To verify the results of the numerical analysis, the conditions assumed must be realized in the test setup. In the analysis a sinusoidal forcing function with constant amplitude is used. The force is configured such that only one mode is excited and the other ones are isolated. The axial force is constant and distributed evenly along the shell circumference. The parameters of the analysis are the excitation level, the axial compressive load, the boundary conditions, and the initial geometric imperfections.

The Requirements of The Test Setup

The following conditions employed in the analysis, were to be realized in the test setup:

1. The axial compressive loads must be distributed evenly along the shell circumference.

2. The excitation system must deliver sinusoidal driving forces with constant amplitudes within each frequency range of interest. The force levels must be sufficiently high to let the shell vibrate in the nonlinear region. The forces must excite only the driven mode in order to show the nonlinear coupling between the driven and companion mode.

3. The response measurement system must be able to detect the response in the form of a standing wave as well as a traveling wave.

The parameters of the analysis which were chosen in the measurement were the axial loads and the excitation levels. No attempt was tried to realize different boundary conditions assumed in the analysis to the test objects. The influence of imperfections will be measured in future tests.

The Test Objects and Boundary Conditions

The test objects were thin-walled cylindrical shells made by machining a seamless aluminium tube to specified dimensions. They were manufactured on a mandrel with the aid of an accurately machined steel mould. In the experiments the shell ends were encased in aluminium end rings to enable the application of axial compressive loads. The rings were attached to the shell by placing each shell end into the circular channel of the ring and filling the ring with melting cerrobend which solidifies when cooling down. A firm attachement was obtained since the cerrobend expands slightly during solidification. These boundary conditions were approximated as C4-C4. **Figure 5** shows the sectional views of this assembly.

Before assembling the shell with the end rings, the wall thickness of the shell was measured at 50 points distributed evenly at 5 axial and 10 circumferential positions. The shell averaged thickness was 0.253 mm with a maximum deviation of 0.007 mm. After the end rings were assembled, the imperfections of the shell were measured by using a UNIVersal instrument for IMPerfections measurement (UNIVIMP [13]) The imperfections which were expressed in a Fourier series had amplitudes less than 0.05 wall thickness.

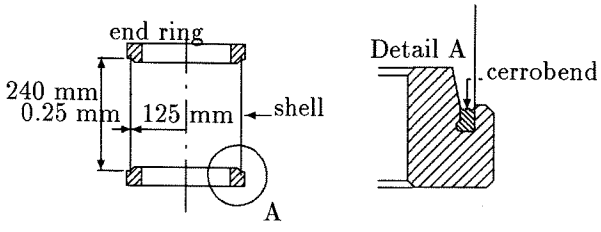

Figure 5: Sectional view of the shell clamped with end rings

The Test Setup

The test objects together with the UNIVIMP were installed in a Compression Testing Machine (CTM), by which axially compressive loads could be applied to the shell, as shown in **figure 6**. The vibration measurement system was built around the CTM. **Figure 7** shows the schematic view of the instrumentation. Two acoustic drivers provided acoustic waves which were projected at two circumferential places. Capacitive displacement transducers are used to measure the shell response. The contactless excitation and measurement systems were used to avoid disturbing changes of the vibration characteristics of the shells.

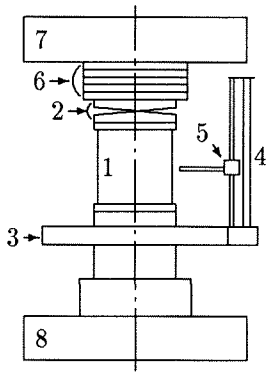

No	Description	No	Description
1	Shell	5	Carriage
2	Top bearing	6	Wooden discs
3	Hexagonal platform	7	CTM upper plate
4	Vertical column	8	CTM lower plate

Figure 6: Shell in the CTM

The Excitation Systems Two self-built acoustic drivers were used to excite the shell. Each driver incorporated a loudspeaker and an exponential horn to concentrate the acoustic waves to a small area on the shell's surface. With an outlet diameter 2.5 cm the horn could effectively excite the vibration modes with circumferential full waves number less than 15 (half wave length larger than 2.6 cm).

To each horn a microphone was flush-mounted close to its outlet to measure the excitation pressure. The distance between horn end and the microphone was 1 cm, and between horn end and the cylinder was 1 mm. Hence the microphone did not measure the actual excitation pressure but the presure at 1.1 cm away from the shell surface. Since the measurements were performed on a vibration mode with natural frequency about 550 Hz, corresponding to a pressure wave length of 65 cm, the errors, however, were not significant.

A pressure synchronizer controlled the phase difference between the pressures of both horns, 0 deg or 180 deg depending on the vibration mode being examined. It also kept the amplitudes of the pressures constant within the frequency range of interest. The phase difference of 0 deg was regulated by

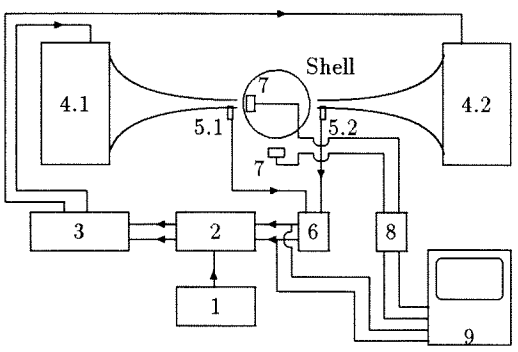

No	Description	Type
1	Wave generator	Prodera GN484
2	Excitation synchronizer	Self built
3	Power amplifier	SA120
4.1	Acoustic exciters no.1	Self built
4.2	Acoustic exciters no.2	Self built
5.1	Microphones no.1	BK4160
5.2	Microphones no.2	BK4160
6	Microphone preamplifiers	BK2633
7	Displacement transducers	$\mu\epsilon$ 600-3
8	Signal conditioners	$\mu\epsilon$ series 600
9	FFT analyzer	DIFA FA100

Figure 7: Schematic View of The Vibration Tests Instrumentation

minimizing the phase difference between the pressure signals of both microphones, and the phase difference of 180 deg by minimizing the pressure signal of microphone 1 and the reversed pressure signal of microphone 2.

Response Measurement Systems Two noncontacting transducers of capacitive type were used to measure the response. The first transducer was placed inside the shell excactly opposite to the excitation point and the second one outside the shell on the carriage of the UNIVIMP which enabled the measurement of response at a variable position. The first transducer in principle measured the amplitude of the driven mode response. The second transducer was used to measure the amplitude of the companion mode response by positioning it at the node of the driven mode response. The accuracy of the transducer is 0.6 μm or 0.003 wall thickness.

Design of the Acoustic Driver

During the preparation of the test setup, the main attention was paid to the design of the acoustic driver. **Figure 8** shows the schematic view of the acoustic driver. It consists of a loudspeaker with an exponential horn and a replaceable tube to concentrate the sound pressure to a small surface on the shell. The back side of the speaker was closed with damping material to avoid box resonance which can lower the sound pressure inside the horn. To provide a large excitation level, the performance of the driver could be optimized by choosing the length of the tube so that the resonant frequency of the air inside the horn was tuned to the natural frequencies of the shell. The design was supported by a mathematical model with the length of the horn and the width of the gap between horn and shell as the parameters.

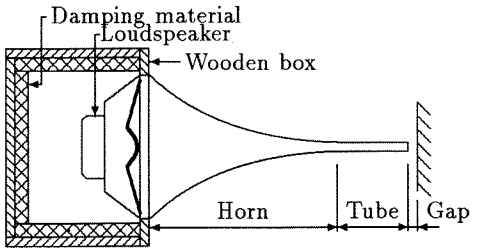

Figure 8: Sectional view of the acoustic driver

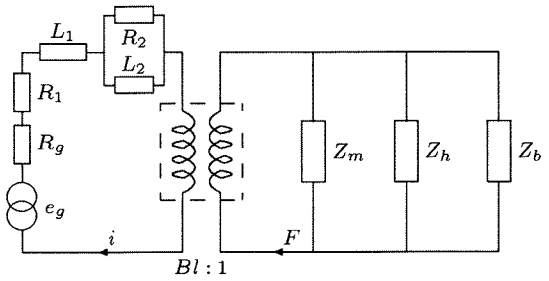

Figure 9: Electrical analogon of the acoustic driver

Figure 9 shows the model as an electrical analogon with e_g is the driving voltage, R_g is amplifier impedance, R_1 is coil resistance, L_1 is losless coil inductance, L_2 is coil inductances with loss R_2, and Bl is the field-strength voice coil length product. The impedance of the loudspeaker cone Z_m is function of cone stiffness, mass and resistance. The impedance of the air from horn side Z_h is a function of horn geometry (length, flare constant), air properties and impedance at the outlet of the horn which depends on the reflection of the test object and the radiation losses via the gap between horn and test object. The impedance of the air from the box side, Z_b, was modelled as an additional stiffness to that of the loudspeaker. By using the parameters of the loudpeaker and the amplifier as supplied by the manufacturers, the loudspeaker pressures at the horn and box sides were calculated. The pressure at the horn outlet was found from the pressure field equation.

4. Small Amplitude Response Measurements

At first the vibration tests were performed for small shell response amplitudes to identify the linear vibration characteristics of the shell, i.e. the resonant frequencies and the corresponding mode shapes.

To identify the resonant frequencies and the corresponding mode shapes in a certain frequency range, frequency response functions (FRF) were measured, i.e. the shell responses at various positions with respect to the excitation force with variable frequency. For this test only a low response level was needed to maintain linearity of the response. Therefore only one driver was used and the excitation synchronizer was inactivated. A chirp was used as excitation signal which permitted the measurement of an FRF within a frequency range in one single sweep.

The driver outlet was positioned at axial position x=4 cm which in principle enabled the excitation of all vibration modes. The linearity of the response was checked by comparing the FRF's measured with different excitation levels. **Figures 10.a, b and c** show the FRF's measured in the frequency ranges 400-800 Hz, 750-1150 Hz and 1100-1500 Hz, respectively. For each frequency range the FRF's, measured by using a driver input signal in the form of a chirp with amplitudes 0.13V, 0.18V and 0.26V, were plotted. No significant differences between the measured FRF's appeared, which indicates the linearity of the response. The measured maximum response level was less than 0.1 wall thickness.

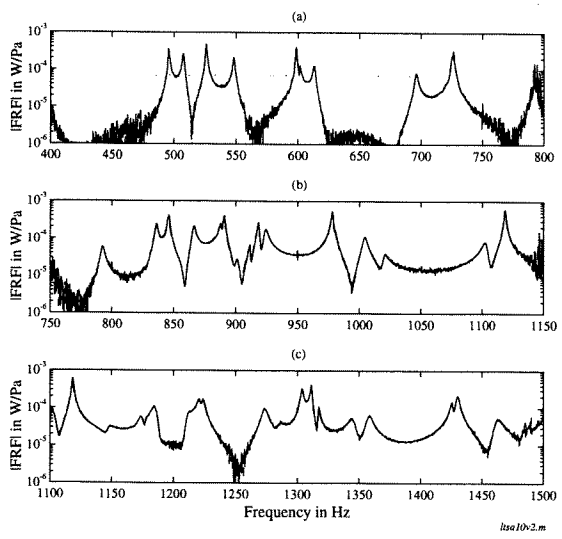

Figure 10: FRF's of a point on the shell surface in three frequency ranges

Sixty-two FRF's were measured, 51 from the points evenly distributed along half of the shell circumference at axial position x=20 cm, and 11 points equally spaced along a line in longitudinal direction. The 62 FRF's were curve-fitted simultaneously by using an iterative multi-curve fit procedure proposed by Goyder [10]. The resonant frequencies were then plotted against the circumferential wave number of the corresponding mode shape, see **figure 11**.

The results may contain some errors due to the high sweep rate of the chirp excitation [8]. Some peaks of the measured FRF were checked by using sinewave excitation. By manually varying the excitation frequency, peak responses occurred slightly to the left of the peaks of the measured FRF. With maximum deviation of about 2 Hz, the FRF were assumed to be sufficiently accurate for the identification purpose.

An interesting phenomenon was observed from the results. Despite the small imperfections of the shell, some modes preferred a spatial position. This turned out for modes (1,6) and (1,7) with axial half wave number m=1. Due to the spatial preference, the response of these modes at the excitation point was not a pure antinode whereas for other modes with no preference the response at the excitation point was always the maximum.

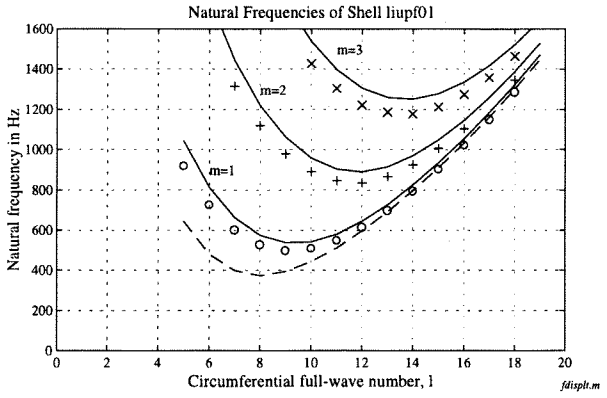

Figure 11: Natural frequency versus circumferential wave number. Circles, plusses and crosses denote modes with m=1, m=2 and m=3, respectively. Calculated results are indicated by solid lines (C4 boundary conditions) and a dashed line (SS3, only for m=1)

A comparison of the measured natural frequencies with the calculated ones was carried out by using the computer program developed by Jansen [5]. The theoretical linear natural frequency in figure 11 is indicated with solid lines for the C4-C4 boundary conditions. For SS3-SS3 boundary conditions the theoretical frequency were calculated only for m=1 and shown with a dashed line. The measured frequencies are close to the calculated ones with C4-C4 boundary conditions as expected. However significant deviations are observed especially at low frequencies.

For the mode (1,11) which was used for the non-

linear vibration tests, the calculated natural frequency is 580.2 Hz and the measured one is 550 Hz. It can be shown that the errors in the natural frequency due to neglecting in-plane inertia and the use of Donnell's theory are small for this mode. Based on approximate expressions in [17] they are estimated to be 0.4 % and 0.6 %, respectively.

Based on the small amplitudes of the measured imperfections, their effect on the natural frequency of mopde (1,11) is expected to be small. A calculation which includes the effect of shell imperfections gives a reduction no larger than 0.2% [12].

The discrepancy between the calculated and measured natural frequency is attributed to the boundary condition of a fully clamped edges not being realized in the experiment, i.e. the clamping via cerrobend could not completely force the displacements u and v and the rotation $W_{,x}$ to be zero at the shell edges. It is known from numerical experiment [14] that the boundary conditions affect the natural frequencies most significantly by constraining the axial displacements. Hence, an axial elastic boundary condition which correlates the state of stress and displacement has been used, $N_x + k_u u = 0$, where k_u is a stiffness parameter, to fit the theoretical to the experimental results. A trial and error procedure suggested the use of stiffness parameter $k_u = 5.10^4 N/m^2$ which gave natural frequency of 544 Hz.

The tests for mode (1,11) were performed at several axial load levels. The natural frequencies at these load levels are given in table 1 where they are compared with the theoretical values using the elastic boundary condition determined for zero axial load. It can be shown that the prediction by using the elastic boundary conditions gives satisfactory results.

Axial Load	Natural Frequency(Hz)	
kN	Calculated	Measured
0.0	544	549
0.75	538	541
2.0	528	531
4.0	512	515
6.0	494	493

Table 1: Natural frequencies of mode (1,11) for different axial loads

5. Large Amplitude Response Measurements

For the large response measurements, the vibration mode (1,11) was used. This mode is well separated from the neighboring modes and has no spatial preferences. To provide a high excitation level two exciters were used. The excitation points were at mid axial position opposite to each other. The drivers were fed with the same sine wave signal and their outputs were controlled to have 180 degrees phase difference.

The sine wave signal was provided by the Prodera sweep sine generator. This generator was programmed such that it stopped the sweep at a certain frequency for a certain period, sent a trigger pulse to the FFT analyzer which then started to record the data signals with time window T. To allow the measurement of the steady state response, a delay time was set in the analyzer which forced the analyzer to make records Δt after receiving a trigger pulse from the generator. After a stop period which was set larger than $T + \Delta t$, the generator jumped to another frequency and repeated the same procedure. To avoid leakage errors in the Fourier transforms of the excitation and response signals, the stop frequency was chosen such that the sampled signals were periodic within the time window of the FFT Analyzer.

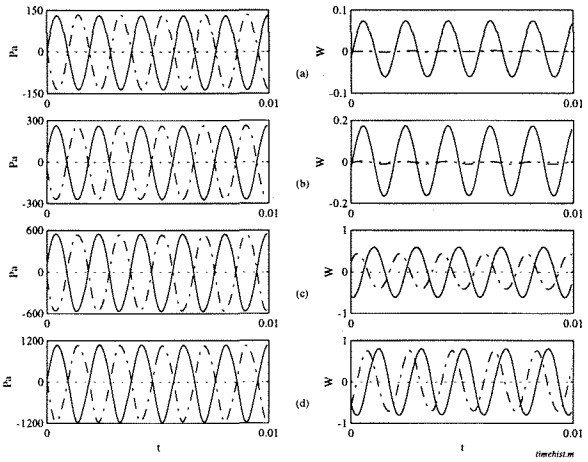

Figure 12: Time records of the pressure (left) and response signals (right) for excitation level (a) 133 Pa,(b) 266 Pa,(c) 533 Pa, and (d) 1066 Pa at 525 Hz. For left figures, the solid and dashed lines are for signals of microphone 1 and 2, respectively while for right figures they are for displacement transducer 1 and 2.

The excitation systems worked properly. **Figure 12** shows the time records of the microphone and displacement transducer signals for 4 different excitation levels at 525 Hz. It can be seen that the pressures had reasonable sinusoidal form with 180 deg phase difference. For the lowest excitation level, the second harmonic content of the pressure is 0.5% and for the highest one 5%. **Figure 13** shows that the transform of the highest excitation pressure in the frequency domain.

The excitation synchronizer could keep the phase difference and amplitudo ratio of 1 within the frequency ranges of interest. **Figure 14** shows the amplitude of excitation pressure of horn 1, ratio between amplitude of excitation pressure 2 and 1, and their

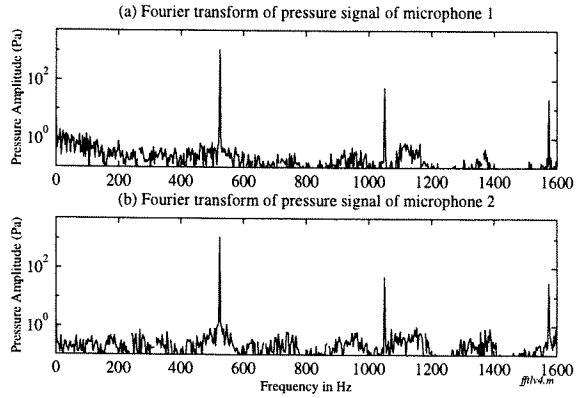

Figure 13: FFT transforms of excitation pressures of both horns at 525 Hz for excitation level 1066 Pa

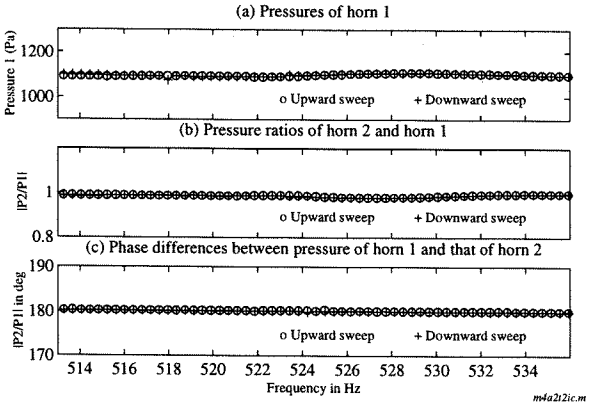

Figure 14: Amplitude and phase relations between pressure of horn 1 and that of horn 1 between 513 and 535 Hz

phase difference from 513 to 535 Hz. This data is depicted from response measurement of shell with 2 kN axial loads and excitation pressure 1066 Pa which by assuming constant pressure distribution over horn outlet corresponds to 0.065 N.

For the axial load level of 2 kN characteristic results are depicted in **figure 15**, where the measured response curve is shown for a high excitation level. The responses for the upward and downward frequency sweep are denoted by circles and plusses, respectively. The jump phenomena corresponding to the nonlinearity occurred. In a small region near the resonant frequency the companion mode responds with amplitudes of the same order of magnitude as the driven mode. Earlier theoretical analyses [3, 9, 15], have predicted a coupled mode response peak due to the appearance of the companion mode, however in the experiment the slope of the driven mode response curve does not show a radical change when the companion mode occurs. Further, in the coupled mode response region, a jump occurs in the response which has not been predicted by earlier theoretical analyses. An examination of the mode shapes before and after this jump shows that the mode has moved to another circumferential position as shown in **figure 16**. The circles denote the response with time phase equal to the response at the excitation point (circumferential position $\theta = 0$ degrees) and the plusses denote the response with 90 degrees phase difference. As a result, the response below the jump frequency was not measured at the maximum amplitude, and the effective excitation level has decreased.

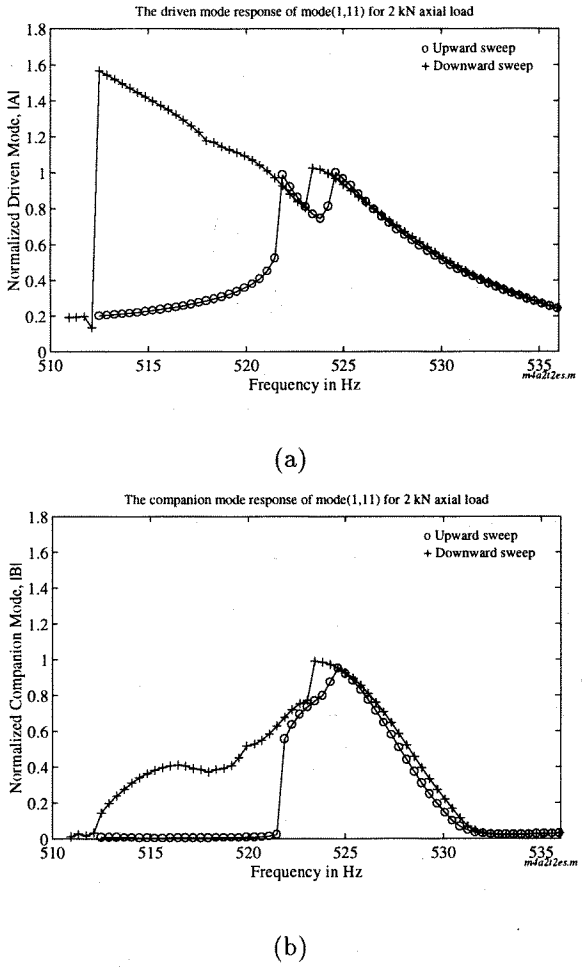

Figure 15: Measured response of mode (1,11) for excitation pressure 1066 Pa with axial load 2kN, a) driven mode, b) companion mode

In **figure 17**, the calculated response is shown for an axial load level of 2 kN [12]. The excitation level corresponds to the excitation pressure used for figure 15, the damping level to the experimentally determined damping for small vibrations (critical damping percentage $\zeta = 0.23$ %). The companion mode appears and vibrates with an amplitude comparable with the driven mode amplitude (of the order of one

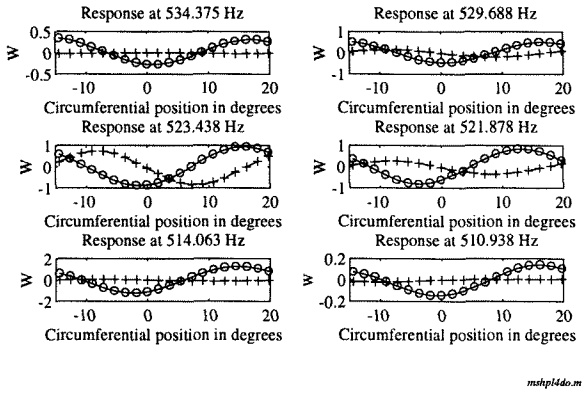

Figure 16: Response distribution of mode (1,11) at several frequencies for excitation pressure 1066 Pa with axial load 2kN during sweep down

wall thickness). Further, the analysis predicts a coupled mode response peak. In a small region, modulated responses in the coupled mode occur and the maximum amplitudes during this beating are indicated by the "driven mode 2" and "companion mode 2" in figure 17). It is noted that the upper branch of the single mode response is unstable at frequencies below the coupled mode response region.

Characteristic time responses of the driven and the companion mode recorded during sweepdown at (a) 534 Hz, (b) 525 Hz, (c) 517 Hz, and (d) 512.5 Hz are shown in **figure 18**. Above the natural frequency, a steady state single mode response occurs. Slightly below the natural frequency the companion mode participates in a steady state coupled mode response. After the jump, the companion mode decreases (with decreasing frequency). In this region, modulated responses are observed.

The influence of the axial compressive load on the response curves is shown in **figures 19 to 21**. The theoretical backbone curves, i.e. the curves for free vibration, for single mode response are based on an perfect shell and on a constant axial load. The phenomena discussed for the case of 2kN were also found at the other axial load levels. The softening behavior is illustrated by the responses for several excitation levels. The 5 excitation levels in figs. 19 and 20 correspond to an excitation pressure in each horn of 67 Pa, 133 Pa, 266 Pa, 533 Pa and 1066 Pa, respectively. In figure 21 the 4 excitation levels correspond to the last four levels. The theoretical backbone curve for single mode response also indicates a softening behavior, but for increasing excitation the corresponding linear frequency seems to decrease in the experiment. Whether this is due to a shift of the mode in circumferential direction or to other effects remains to be investigated.

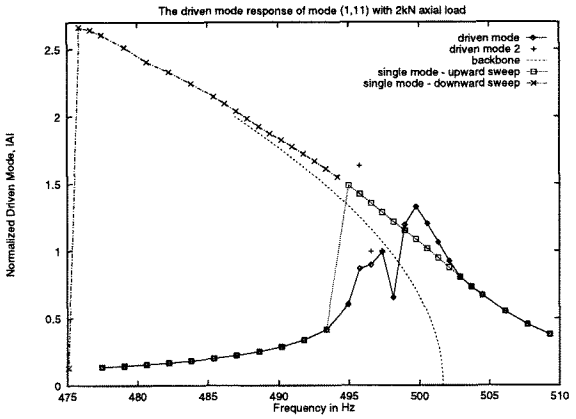

(a)

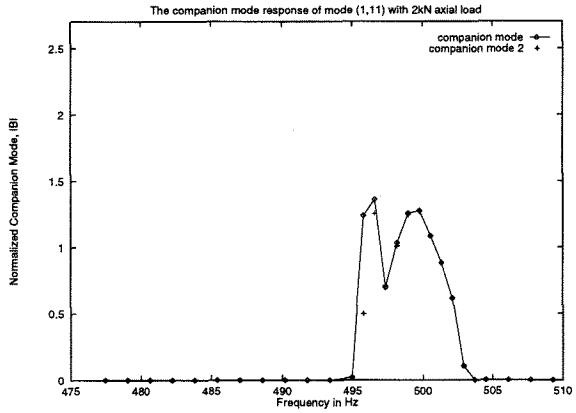

(b)

Figure 17: Calculated response of mode (1,11) for excitation level $Q_{mlr} = 22$ Pa with axial load 2kN, a) driven mode, b) companion mode

6. Conclusions

A setup for experimental nonlinear vibrations of cylindrical shells has been built. The setup fulfilled the requirements which is needed to make the measurement results comparable to the analysis.

The measurement results approved the theoretical results. A weak nonlinearity of a softening type was found and in the frequency range around resonance a response in the form of traveling waves was measured. Increasing axial compressive load make the natural frequencies shift to lower values. However the nonlinear behavior of the shell, i.e. the softening nonlinearity and the occurrence of the traveling wave responses does not alter.

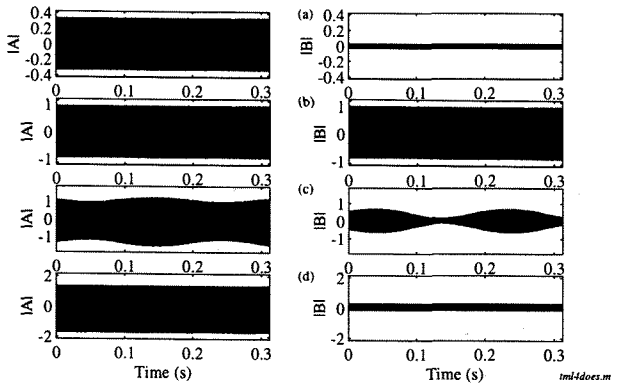

Figure 18: Time history of the response of mode (1,11) for excitation pressure 1066 Pa with axial load 2kN during sweep down for driven mode (left) and companion mode (right) at (a) 534 Hz, (b) 525 Hz, (c) 517 Hz and (d) 512.5 Hz.

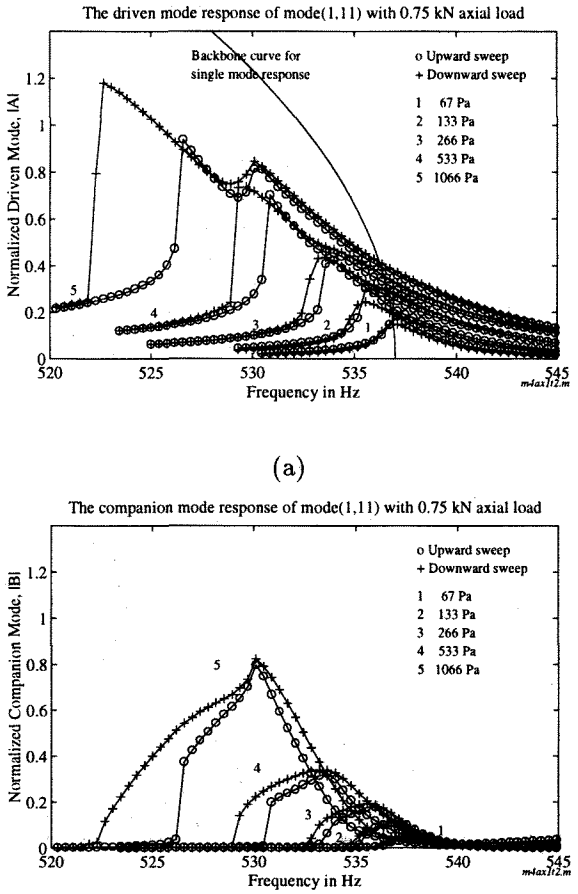

Figure 19: Measured response of mode (1,11) with axial load 0.75 kN for several excitation levels, a) driven mode, b) companion mode. Theoretical backbone curve is shown for single mode response

References

[1] L.L.Beranek, Acoustics, McGraw Hill Book Co., New York, 1954.

[2] M.M.Boone, D.de Vries, A.J.Berkhout, Sound Control part 1&2, Faculty of Applied Physics, Delft University of Technology, The Netherlands, 1991.

[3] J.C. Chen and C.D. Babcock, Nonlinear Vibrations of Cylindrical Shells, AIAA Journal, 13(7)(1975), pp.868-876.

[4] H.N.Chu, Influence of Large Amplitudes on Flexural Vibrations of a Thin Circular Cylindrical Shell, J.Aerospace Sci., 28(8), 1961.

[5] E.L. Jansen, Nonlinear Vibrations of Composite Cylindrical Shells, PhD Thesis, Delft University of Technology, Faculty of Aerospace Engineering, Delft, to appear in 1996.

[6] D.A.Evensen, A theoretical and Experimental Study of the Nonlinear Flexural Vibrations of Thin Circular Rings, NASA TR R-227, 1965.

[7] D.A.Evensen, Nonlinear Flexural Vibrations of Thin-walled Circular Cylinders, NASA TN D-4090, 1967.

[8] D.J.Ewins, Modal Testing: Theory and Practice, Research Studies Press Ltd., England, 1986.

[9] J.H. Ginsberg, Large Amplitude Forced Vibrations of Simply Supported Thin Cylindrical Shells, ASME Journal of Applied Mechanics, 40(1973) pp.461-477.

[10] H.G.D.Goyder, Methods and Application of Structural Modelling from Measured Structural Frequency Response Data, J.Sound and Vibration 68(2), p209-230, 1980.

[11] L. Gunawan, Vibration Tests of Shell Liupf01, LR-report, Delft University of Technology, Faculty of Aerospace Engineering, Delft, to appear in 1996.

[12] L. Gunawan, E.L.Jansen, Nonlinear Vibrations of Cylindrical Shell under Axial Compressive Loading, ESTEC96 Conference, Noordwijk, The Netherlands, 1996.

[13] A.W.H.Klompé, UNIVIMP, A Universal Instrument for The Survey of Initial Imperfections of Thin-walled Shells, Report LR-570, Faculty of Aerospace Engineering, Delft University of Technology, The Netherlands, 1988.

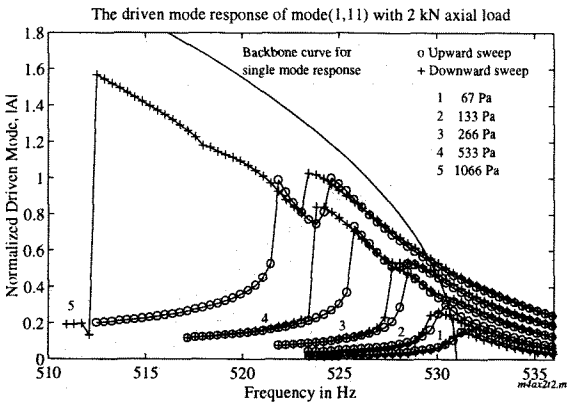

(a)

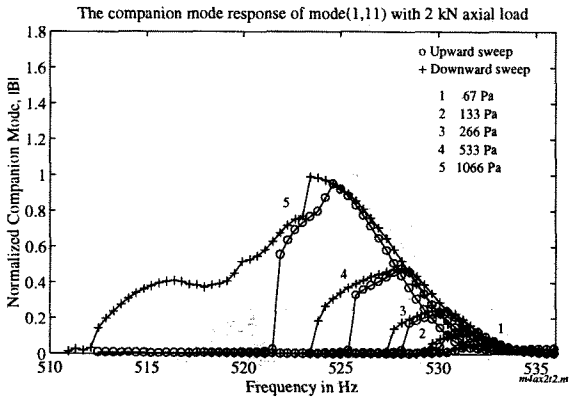

(b)

Figure 20: Measured response of mode (1,11) with axial load 2 kN for several excitation levels, a) driven mode, b) companion mode. Theoretical backbone curve is shown for single mode response

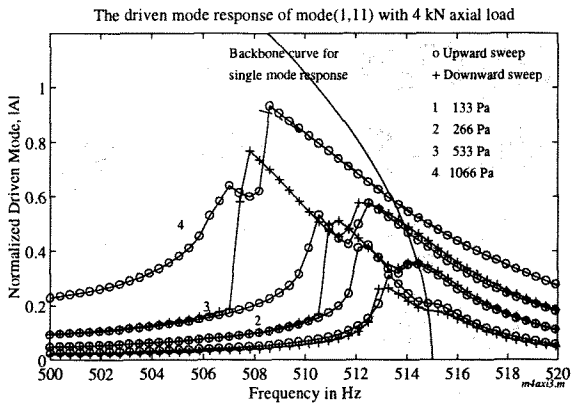

(a)

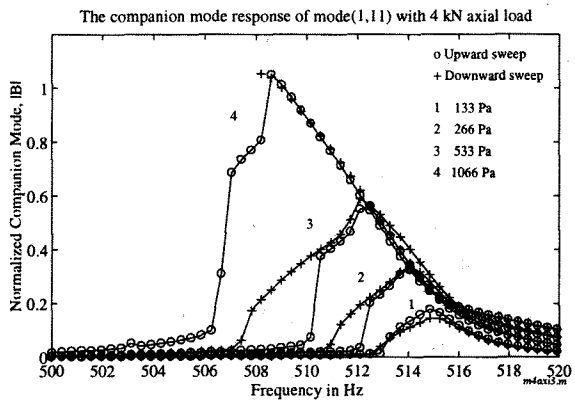

(b)

Figure 21: Measured response of mode (1,11) with axial load 4 kN for several excitation levels, a) driven mode, b) companion mode. Theoretical backbone curve is shown for single mode response

[14] T.Koga, Effects of Boundary Conditions on the Free Vibrations of Circular Cylindrical Shells, AIAA Journal 26(11),p.1387-1394, 1988.

[15] D.K.Liu, Nonlinear Vibrations of Imperfect Thin-walled Cylindrical Shell, Doctoral Thesis, Delft University of Technology, Faculty of Aerospace Engineering, Delft, 1988.

[16] D.K.Liu, Survey and suggestions for experiments of nonlinear vibrations of thin-walled cylindrical shells, Report LR-458, Dept.of Aerospace Engineering, TUDelft, The Netherlands, 1985.

[17] W.Leissa, Vibration of Shells, NASA SP-288, 1973.

[18] J.L.Nowinski, Nonlinear Transverse Vibrations of Orthrotropic Cylindrical Shells, AIAA Journal 1(3), p.617-620, 1963.

[19] D.de Vries, M.M.Boone, C.P.A.Wapenaar, Inleiding in de Akoestiek, Lecture Notes, Faculty of Applied Physics, Delft University of Technology, The Netherlands, 1991.

[20] K.J.J.M.Zaal, An Experimental Invesigation of the Nonlinear Vibrations of Thin-walled Cylindrical Shell, Master Thesis, Delft University of Technology, Faculty of Aerospace Engineering, Delft, 1989.